Journal of the European Ceramic Society 38 (2018) 4057–4063

Contents lists available at ScienceDirect

Journal of the European Ceramic Society

journal homepage: www.elsevier.com/locate/jeurceramsoc

Original Article

Preparation of transparent $MgO{\cdot}1.8Al_2O_3$ spinel ceramics by aqueous gelcasting, presintering and hot isostatic pressing

He Zhang[a], Hao Wang[a,*], Honggang Gu[b], Xiao Zong[a], Bingtian Tu[a], Pengyu Xu[a], Bin Wang[a], Weimin Wang[a], Shiyuan Liu[b], Zhengyi Fu[a]

[a] State Key Lab of Advanced Technology for Materials Synthesis and Processing, Wuhan University of Technology, Wuhan 430070, China
[b] State Key Laboratory of Digital Manufacturing Equipment and Technology, Huazhong University of Science and Technology, Wuhan 430074, China

ARTICLE INFO

Keywords:
$MgO{\cdot}1.8Al_2O_3$anti-hydrolysis
Gel-casting
PS/HIP
Transparent ceramic

ABSTRACT

Non-stoichiometric $MgO{\cdot}1.8Al_2O_3$ spinel transparent ceramic was prepared from synthesized single phase powder through an aqueous gel-casting forming technique. In order to prevent hydrolysis, the powder was specially treated in toluene with stearic acid and then dispersed in an aqueous solution with the help of amphoteric compound Tween 80 and dispersant TMAH. The surface modification process was confirmed by various techniques such as Fourier transmission infrared absorption spectroscopy (FT-IR), pH value, zeta potentials and rheological properties. Afterwards, gel-casted green compacts were debinded, pressureless-sintered (PS) and hot-isostatic-pressed (HIP). Highly transparent $MgO{\cdot}1.8Al_2O_3$ ceramics (3.6 mm in thickness) with in-line transmittance values of 77–82 % in visible region and higher than 85% in near infrared region were obtained. The samples exhibited Knoop hardness of 12.2 ± 0.2 GPa, Young's modulus of 302 GPa, refractive index of 1.7046, and Abbe's number of 75.8.

1. Introduction

With the advance of modern technologies, the need for more demanding optical applications has spurred a considerable study interest in transparent polycrystalline ceramics. Transparent polycrystalline ceramics have a unique combination of both excellent optical properties and high mechanical properties not acquired with other materials [1–3]. Furthermore, they can be formed into complex and large-sized near-net shapes at lower cost compared with single crystals. Transparent polycrystalline magnesium aluminate spinel, one of few candidates with high transmittance ranged from ultraviolet (UV) to medium wavelength infrared (MWIR) light and excellent mechanical properties [4], is particularly promising to fill this demand [5,6].

At appropriate temperatures, there exist interstitial cations or cationic vacancies in the spinel lattice and a series of non-stoichiometric $MgO{\cdot}nAl_2O_3$ where n can range from 0.6 (Mg-rich) to 9.1 (Al-rich) [7–9], which results in a wide range of intrinsic properties. For example, the change of Al content in the $MgO{\cdot}1.8Al_2O_3$ spinel can lead to a decreasing lattice parameter compared with $n = 1$ [10,11], which is in accordance with the results of theoretical prediction from Tu et al. [12].

Up to now, most research has focused on $MgAl_2O_4$ ($n = 1$) transparent ceramics for more than fifty years. Nevertheless, in recent years some progress has been made in the research of non-stoichiometric magnesium aluminum spinel $MgO{\cdot}nAl_2O_3$ mainly through reactive hot pressing (HP) [13,14]. According to Krell et al. [10,15], the excess Al in spinel when $n > 1.5$ could promote densification since the Al_2O_3 typically exhibits a higher sintering activity than $MgAl_2O_4$ during reactive sintering. In accordance with that, spinels with n equal to 2 and 2.5 were found to exhibit relatively high optical transmittance (> 82%) at visible wavelength [16]. Moreover, theoretical calculations showed that elastic modulus of Al-rich spinel can be enhanced by increasing Al content [12], which was also supported by the experimental data from Mitchell et al. [17]. It was reported that Al-rich transparent spinel windows do not exhibit the well-known absorption at around 3000 nm commonly relative to the incorporation of hydrogen into the spinel lattice [18,19]. However, the formation of the spinel phase from Al_2O_3 and MgO involves a volume expansion of ~8%, which hinders the densification of spinel ceramics through a single-stage reaction sintering process [20]. Additionally, it is quite difficult to control composition and homogeneity through reaction sintering process for preparing transparent spinels especially with large size and complex shape. Researches have already indicated that above problems could be well solved using synthetic pure single-phase ceramic powder combined with pressureless pre-sintering (PS) and hot isostatic pressing (HIP) [21,22].

* Corresponding author.
E-mail address: shswangh@whut.edu.cn (H. Wang).

https://doi.org/10.1016/j.jeurceramsoc.2018.04.057
Received 10 January 2018; Received in revised form 24 April 2018; Accepted 27 April 2018
Available online 30 April 2018
0955-2219/

The shaping process is the key step for converting powder into desired shapes and vitally important for acquiring ceramics with high homogeneity and transmittance. Near-net-shape forming of ceramics can be achieved by a gelcasting (GC) processing technique, which is of great importance because subsequent expensive post-sintering machining operations can be minimized or even eliminated [23,24]. Furthermore, aqueous processing offers several environmental and economic benefits in addition to the ability to manipulate inter-particle forces in aqueous suspensions [25,26]. Unfortunately, owing to the basic nature of magnesium aluminate spinel powder, the preparation of aqueous suspension becomes rather difficult since the serious hydrolysis reaction tends to coagulate the slurry and limit the practical solid loading to around 30 vol% [27]. As it is known, low solid loading (< 50 vol%) is very likely to result in low green density, low green strength and inhomogeneous structure of green body structure. To solve this problem, on one hand, the powder needs to be treated for anti-hydration. On the other hand, all additives added into the suspensions have to be eliminated after binder burnout for the sake of ultimately obtaining highly transparent spinel ceramics [7].

Ganesh et al. used H_3PO_4 and $Al(H_2PO_4)_3$ as hydration-resistance reagents to passivate $MgAl_2O_4$ powder [28–31]. The passivating treatment can generate compact monomolecular phosphate layers on the surface of powder and inhibit the direct contact between deionized water and powder. Consequently, the hydrolysis phenomenon is mainly eliminated. But one of serious problems of this treatment is that the phosphate layers can hardly be excluded in the subsequent binder removal process. Besides, the introduction of $Al(H_2PO_4)_3$ would make Al content uncontrollable in $MgO{\cdot}nAl_2O_3$ solid solution system. Although the selection of modifier is questionable for preparing transparent spinels, the idea that generates isolation layers on the surface of the powder is advisable. Stearic acid is a common modifier and easily excluded in the subsequent binder burnout, hence it can be considered as the modifier for $MgO{\cdot}1.8Al_2O_3$ powder instead of the above-mentioned H_3PO_4 and $Al(H_2PO_4)_3$. Egashira et al. conducted acid cleaning and passivating treatment of AlN powder with stearic acid, and then prepared slurry with good suspension properties. As a result, pH value of the treated AlN powder remained almost unchanged after contacting with water for 72 h [32].

In this work, fine single-phase $MgO{\cdot}1.8Al_2O_3$ powder with average grain size of ~200 nm was treated for anti-hydration with stearic acid and Tween 80. The feasibility and the related mechanism of this treatment have been studied. Furthermore, green body was formed by gelcasting combined with cold isostatic pressing (CIP) using the treated powder. Highly transparent $MgO{\cdot}1.8Al_2O_3$ spinel ceramics were firstly fabricated from the green body by PS and HIP. The phase composition, surface modification process, some mechanical and optical properties of the specimens were investigated.

2. Experimental procedure

$MgO{\cdot}1.8Al_2O_3$ powder was synthesized by solid-state reaction of 64.29 mol% α-Al_2O_3 (99.99%) and 35.71 mol% MgO (99.95%). The as-synthesized powder was de-agglomerated through ball milling at 250 rpm for 12 h in absolute ethyl alcohol solution. Henceforth, this synthesized non-stoichiometric ceramic powder is termed as NMAS powder. The NMAS powder was specially treated for anti-hydrolysis in toluene (AR, Sinopharm) with stearic acid ($C_{18}H_{36}O_2$, Aladdin, China) in a round-bottomed flask before shaping. The ratio of powder weight (g):toluene volume (ml):stearic acid weight (g) is 100:200:0.3. The slurry was first agitated with a magnetic stirrer (5MLH-DX, Remi, Hyderabad, India) for 55 min, and then, vacuum rotary evaporation was used to remove the excess toluene. Finally the powder was dried at 65 °C for 24 h and sieved (200 mesh sieve). This treated NMAS powder is termed as T-NMAS powder.

With the help of 0.8 wt% polysorbate 80 (Tween 80, $C_{67}H_{128}O_{26}$, Macklin, China) and 1.5 wt% tetramethylammonium hydroxide (TMAH, $C_4H_{13}NO$, Macklin, China), aqueous suspension with 50 vol% solid loading was prepared by dispersing the T-NMAS powder in an aqueous premix solution containing 20 wt% methacrylamide (MAM, Urchem, China) and 2 wt% methylenebisacrylamide (MBAM, Alfa Aesar, UK) in deionized water. The suspension was stirred for 6 h in a beaker, then degassed for 5 min under partial vacuum to remove bubbles. The suspension was once again degassed for 25 min after introducing 1.0 vol% polymerization initiator (10 wt% aqueous solution of ammonium persulfate (APS, $H_8N_2O_8S_2$, 98%, Alfa, China)). After added 0.5 vol% tetramethylethylenediammine (TEMED, 99%, $C_6H_{16}N_2$, Alfa, China), the suspension was stirred slowly and cast into a non-porous steel mold. The as-consolidated green body was demolded after stored for 24 h in the steel mold at room temperature. Then, the as-demolded green body (ϕ 20 × 4.8 mm) was slowly dried for 24 h in air, and further dried at 100 °C for 10 h with a heating rate of 0.5 °C/min. The obtained green body was CIP-ed (LDJ320/700-400, Sichuan, China) for 5 min at 200 MPa. Subsequently, the CIP-ed green body was heated up to 630 °C at a heating rate of 1 °C/min in a muffle furnace for the purpose of binder burnout. For comparison, another green body (ϕ 20 × 2.5 mm) was also fabricated by dry pressing (DP) followed by CIP (200 MPa/5 min) of untreated single-phase $MgO{\cdot}1.8Al_2O_3$ powder. The obtained debinded GC body and DP body were firstly pressureless-sintered at 1700 °C for 2 h in nitrogen atmosphere, and then fully densified by HIP at 1880 °C for 5 h under argon pressure of 180 MPa. At last, the sintered GC sample (ϕ 16 × 3.8 mm) was ground and polished to 3.6 mm in thickness.

Phase composition of NMAS powder and sintered ceramics was determined by X-ray diffraction (XRD, X'Pert PRO of Panalytical, Netherlands). Microstructure and particle size of NMAS and T-NMAS powders were characterized by scanning electron microscopy (SEM, S-3400, Hitachi, Tokyo, Japan). Fourier transmission infrared absorption spectroscopy (FT-IR, Thermo Nicolet 6700, Thermo Nicolet Corporation, Washington, USA) was used to characterize functional groups of both NMAS powder and T-NMAS powders. A UV–vis spectrophotometer (Lambda 750 S, PerkinElmer, USA) (0.2–2.5 μm) and a FT-IR spectrometer (2.5-25 μm) were used to measure the in-line transmission spectra of sintered samples. pH value measurement was performed using a digital pH meter (AS600, As One Corporation, China). Zeta potentials of the dilute solutions of NMAS and T-NMAS powders were determined by Zetaplus analyzer (Zetaplus, Brookhaven, USA) using an electrophoretic light-scattering method at 25 °C. 1 mmol/L NaCl solution was used as solvent and the powder concentration was maintained at 0.05 vol%. Rheological behavior of the slurry for gelcasting was characterized by a rotational rheometer (Brookfield Viscometer, USA) at a shear rate ranging from 0.01 s^{-1} to 56 s^{-1}. Pore size distribution of the green body was evaluated by an automatic mercury porosimeter (AutoPore IV95/0, Shanghai, China). The density of sintered samples was measured following Archimedes method (GB/T 25995-2010, China). The relative density of pre-sintered and sintered samples was calculated based on theoretical density of 3.635 g/cm^3, and the relative density of green bodies before PS was evaluated by the automatic mercury porosimeter. Knoop hardness of ceramic samples was recorded by a hardness tester (Model 430SVD, Wolpert, China) at a load of 1 kg for 15 s. Young's modulus was measured by a digital oscilloscope (TDS2022C, Tektronix, China) and an ultrasonic pulse generator (5072PR, Olympus, Japan). In each single experiment of Knoop hardness and Young's modulus the average was determined from 8 valid data, and the standard deviations of these 8 primary data per sample were calculated. Refractive index and dispersion of GC samples were measured by a spectroscopic ellipsometer (ME-L, Wuhan Eoptics Technology Co., Ltd, China) [33,34]. In the ellipsometric analysis, the dispersive properties of the optical constants were described by Cauthy model, and a Bruggeman EMA layer (that contains 50% sample and 50% void) with a thickness of about 3.76 nm was introduced to account for the surface roughness of the sample.

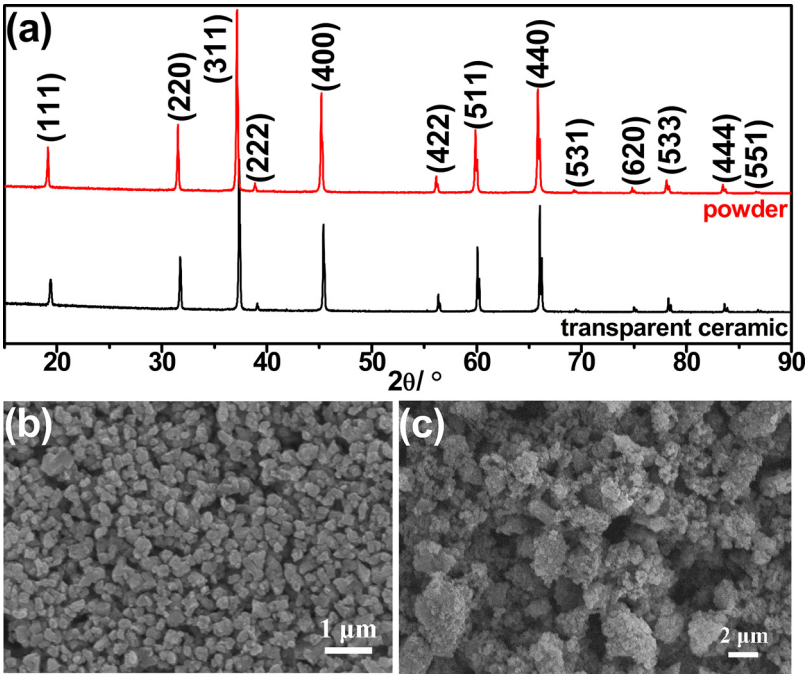

Fig. 1. (a) XRD patterns of synthesized $MgO{\cdot}1.8Al_2O_3$ powder and transparent ceramic. (b) Morphology of ball milled $MgO{\cdot}1.8Al_2O_3$ powder. (c) Morphology of ball milled $MgO{\cdot}1.8Al_2O_3$ powder after contacting with water for 72 h at room temperature.

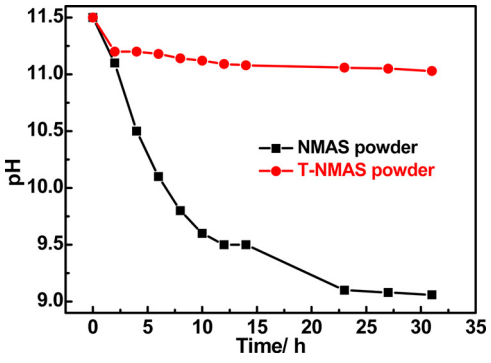

Fig. 2. Change in pH value with time for the untreated NMAS and anti-hydration T-NMAS powders (Experimental conditions: 50 vol% solid loading, static condition at room temperature).

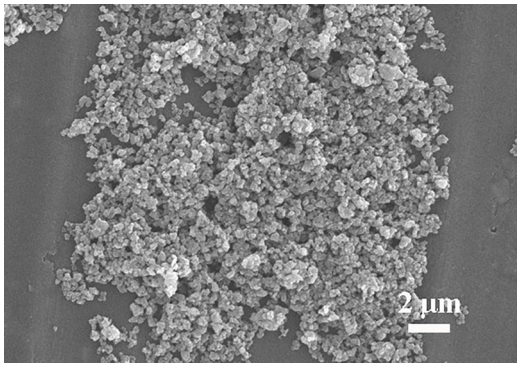

Fig. 4. Morphology of treated $MgO{\cdot}1.8Al_2O_3$ powder after immersion in water for 72 h at room temperature.

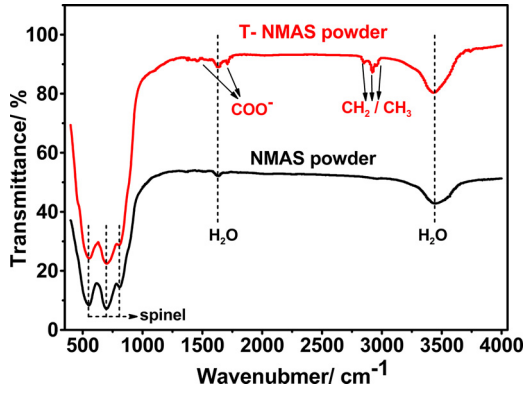

Fig. 3. FTIR spectra of NMAS and T-NMAS powders.

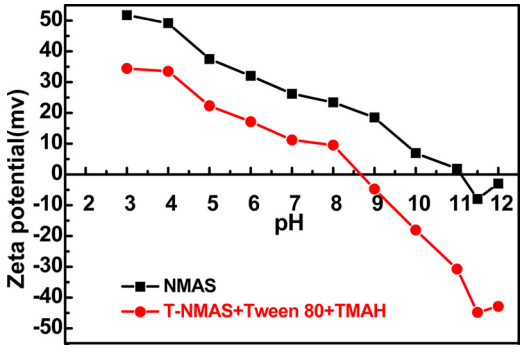

Fig. 5. Zeta potentials versus pH of the as-synthesized (NMAS) and the surface treated (T-NMAS) powders with the help of Tween 80 and TMAH.

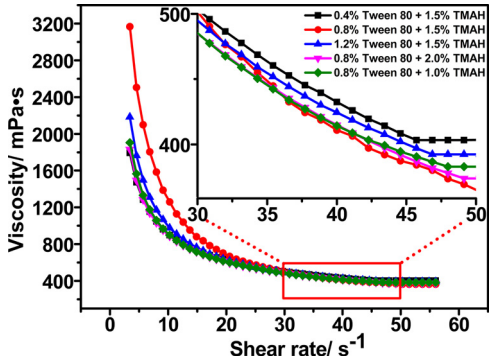

Fig. 6. Viscosity versus shear rate of the aqueous suspensions containing different contents of Tween 80 and TMAH. The inset is the partial enlarged picture of the viscosity versus shear rate ranging from 30 s^{-1} to 50 s^{-1}.

3. Results and discussion

3.1. Characteristics and surface treatment of NMAS powder

High-purity single phase $MgO{\cdot}1.8Al_2O_3$ powder was obtained as shown in Fig. 1a. After sintering, there is no secondary phase observed in the transparent ceramic. Fig. 1b indicates that the as-synthesized $MgO{\cdot}1.8Al_2O_3$ powder has a uniform particle size distribution. However, it can be seen from Fig. 1c that particles have a strong agglomeration after being contacted with water, which could lead to serious sedimentation when preparing slurry.

It is generally accepted that the film on the surface of magnesium aluminate spinel powder exists in the form of AlOH and MgOH groups, which is commonly considered as the main reason for hydrolysis [29]. The possible reason for the sedimentation is that hydrolyzed particles tend to agglomerate due to the cement properties of MgOH groups. In order to prepare stable slurries containing no less than 50 vol% solid loading, the powder was specially treated in toluene with stearic acid (R-COOH). The AlOH and MgOH groups on the surface of particles played an important role in the formation of an isolated protective layer against water by undergoing polycondensation reaction between −OH and −COOH. Although the obtained powder through above surface treatment achieved the purpose of anti-hydrolysis, they were no longer hydrophilic. In order to obtain the enough dispersion ability in aqueous solution, the T-NMAS powder needs to be treated with an amphoteric surfactant Tween 80 and a dispersing agent TMAH [35].

Fig. 2 shows the change in pH value with time for NMAS and T-NMAS powders. As illustrated, the pH value of slurry with untreated powder had a great change from 11.5 to 9.1 after 31 h. However, the pH value of slurry with surface-modified powder still remained almost unchanged even after 31 h. This result confirms the effectiveness of modification. The slight decrease in pH value for both NMAS and T-NMAS powders during first several hours might be due to the volatilization of ammonia derived from the pH adjustment agent.

Fig. 3 shows FT-IR spectra of NMAS and T-NMAS powders recorded between 400 and 4000 cm^{-1}. Broad bands in the region at around 3435 cm^{-1} and 1631 cm^{-1} of both NMAS and T-NMAS powders correspond to −OH stretching and H−O−H bending vibrations of water adsorbed, respectively. Water can be easily distinguished from hydroxyl groups by the presence of the H−O−H bending motion, which also produced a medium band in the 1600–1650 cm^{-1}. Free water has a strong and broad absorption band centered in the region around 3400 cm^{-1} [36]. As it is known, water is easily introduced with KBr during the sample preparation. Hence, the existence of absorbed water in the treated powder may be due to the hygroscopicity of KBr. The absorption bands at around 546 cm^{-1}, 700 cm^{-1} and 808 cm^{-1} correspond to γ_2, γ_1 and γ_5 of magnesium aluminate spinel, respectively [37,38]. As shown in FT-IR spectrum of the T-NMAS powder, large absorption bands at 2800–3000 cm^{-1} due to characteristic vibrations of stearic acid indirectly validate the successful M-OOC-R coating on the surface of the powder. In addition, the presence of new bands at 1686 cm^{-1} and 1468 cm^{-1} which correspond to the carboxylate ν_{coo-} gives another powerful evidence that acid groups (−COOH) have been transformed into carboxylate groups (−COOR) [39]. Thus stearic acid was successfully bonded to the surface of $MgO{\cdot}1.8Al_2O_3$ spinel particles through the formation of strong chemical bonding. Meanwhile, the absence of bands at about 779 cm^{-1} and 676 cm^{-1} relative to the benzene ring of toluene indicates that the excess toluene was removed by the vacuum rotary evaporation.

As shown in Figs. 1c and 4 , the difference between hydrolysis behaviors of the NMAS and T-NMAS powders after immersion in water for

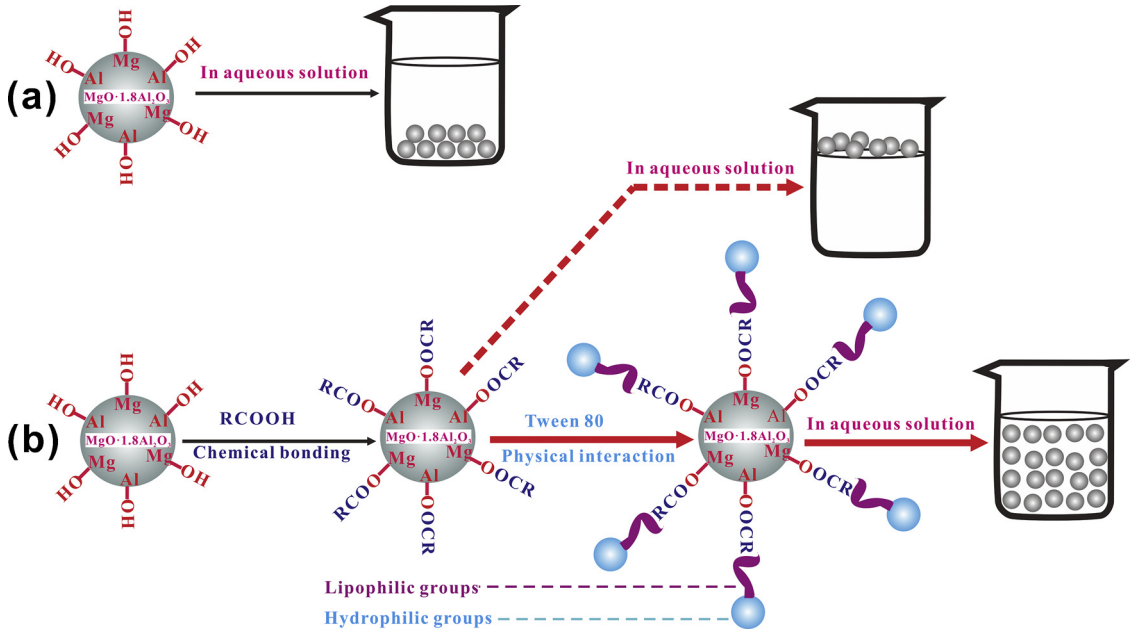

Fig. 7. (a) Hydrolysis phenomenon of the untreated $MgO{\cdot}1.8Al_2O_3$ powders. (b) The whole treatment mechanism schematic diagram (R is the alkyl chain of stearic acid).

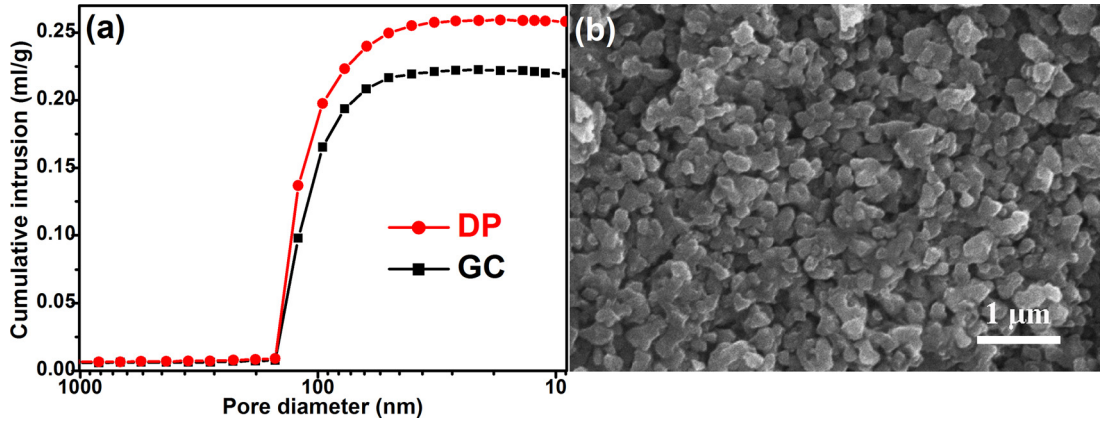

Fig. 8. (a) Pore size distribution of debinded bodies made of T-NMAS powders by gelcasting and NMAS powders by dry pessing, respectively. (b) SEM image of debinded body by gelcasting after cold isostatic pressing (CIP, 200 MPa for 5 min).

Table 1
Properties of green bodies, pre-sintered and HIPed T-NMAS ceramics consolidated by gelcasting. And the properties of green bodies, pre-sintered and HIPed NMAS ceramics by dry pressing is also given in order to make comparison.

Sample	Properties of green bodies before and after CIP	Properties of pre-sintered ceramics		Properties of post-HIPed ceramics		
	Relative density (%)	Linear Shrinkage (%)	Relative Density (%)	Hardness (HK1) (GPa)	Young's Modulus (GPa)	Refractive Index (n_D)
GC	52.1; 56.2 (CIPed)	20.3	98.2	12.2 ± 0.2	302	1.7047
DP	51.4 (CIPed)	19.6	96.8	Not determined	Not determined	Not determined

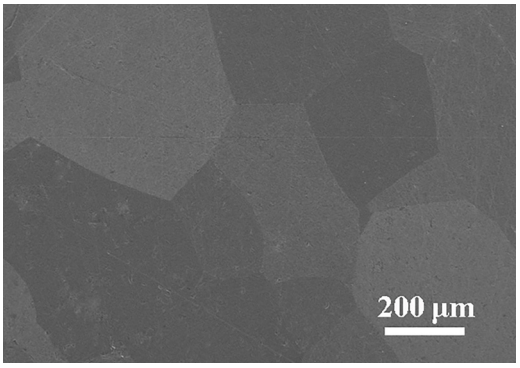

Fig. 9. Microstructure of the acid-etched surface of $MgO{\cdot}1.8Al_2O_3$ transparent ceramic after HIP at 1880 °C for 5 h under argon pressure of 180 MPa.

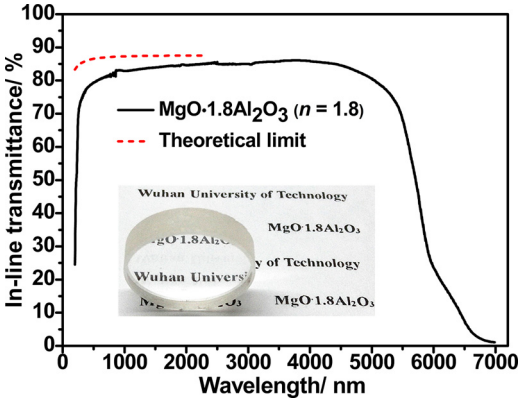

Fig. 10. The in-line transmittance and physical photo of $MgO{\cdot}1.8Al_2O_3$ spinel transparent ceramic (3.6 mm in thickness). The upper line gives the theoretical limit (= $2n/(n^2 + 1)$, with n-refractive index [depending on the wave length]), and the theoretical limit is 87.579% at 1690 nm.

72 h is confirmed by SEM observations. The T-NMAS powder exhibit great hydration-resistance in Fig. 4.

3.2. Characteristics of T-NMAS suspension and green body by aqueous gelcasting

Fig. 5 shows the dependence of zeta potentials (ζ) of the NMAS and T-NMAS powders on pH value. It can be seen that the as-synthesized powder exhibits a pH_{iep} (iep is iso-electric point) of ~10, whereas the treated $MgO{\cdot}1.8Al_2O_3$ powder exhibits a pH_{iep} of ~8.7. The shift of the pH_{iep} confirms that the T-NMAS powder possesses completely different surface chemical properties. Meanwhile, T-NMAS powder dispersed with Tween 80 exhibits negative ζ value in the range of 40–50 mV at pH ≈ 11.5, which ensures the preparation of stable and concentrated aqueous suspension.

The viscosity versus shear rate of aqueous gelcasting suspensions containing 50 vol% T-NMAS powder is shown in Fig. 6. All slurries exhibit shear-thinning behavior. And when the content of Tween 80 and TMAH are equal to 0.8 wt% and 1.5 wt% respectively, the viscosity of the slurry is the lowest, which is more suitable for the following casting process.

All in all, the mechanism schematic diagram is shown in Fig. 7. The mechanism of the modification process is as follow:

Step 1: For the purpose of anti-hydrolysis, a long-chain M-OOC-R (M = Al or Mg) was firstly formed from the chemical reaction between stearic acid (R-COOH) and NMAS powder (M-OH).

Step 2: Lipophilic groups of Tween 80 were integrated with the alkyl chain (-R) of T-NMAS powder (M-OOC-R) by cross-linking effect between organics, and hydrophilic groups of Tween 80 were exposed in aqueous solution.

Step 3: OH^- and large organic cations originated from the ionization of TMAH made Tween 80-treated T-NMAS powder well dispersed in aqueous solutions, and finally stable slurries with solid loading no less than 50 vol% were obtained.

Due to the loss of water during the drying process of GC green body, there exist a lot of connected pores. After CIP process, the relative density of GC green body could be improved. In addition, the

nonuniform drying process of GC sample surface and interior led to inhomogeneity in GC green body [24]. And the homogeneity of GC green body can be enhanced by CIP after drying. Fig. 8a shows pore size distribution of the DP body and debinded GC body, respectively. It is noticed that the total cumulative intrusion in GC body (0.22 ml/g) is smaller than that of the DP body (0.26 ml/g). The average pore sizes of both GC and DP samples are ~100 nm. Based on the cumulative intrusion volume, the relative density of GC and DP green bodies were calculated as 55.6% and 51.4%, respectively. The debinded GC body with high relative density is more advantageous to the preparation of high-quality transparent ceramics [40]. Fig. 8b shows SEM image of debinded GC body. As shown in Fig. 8b, it can be seen that the microstructure structure of debinded GC bodies was uniform.

3.3. Characteristics of sintered T-NMAS body

As shown in Table 1, the relative densities of GC green body and DP green body before and after CIP are given. After CIP, the relative density of GC green body increases from 52.1% to 56.2%, the relative density of DP green body before CIP is not given because the sample with low strength can not be evaluated by automatic mercury porosimeter. Furthermore, the relative density of GC green body is larger than that of DP green body (56.2% vs 51.4%). The reason of difference between 56.2% (GC green body) and 55.6% (debinded GC body) is due to the binder burnout process. The linear shrinkage, relative density of GC sample on pre-sintering are shown in Table 1. It can be seen that the linear shrinkage (20.3%) of GC sample is larger than that (19.6%) of DP sample, and the relative density of GC sample and DP sample after PS are 98.2% and 96.8%, respectively. Meantime, the higher relative density of GC sample indicates that gelcasting process is more likely to obtain consolidated samples.

The Knoop hardness and Young's modulus of GC samples were measured and listed in Table 1 as well. The similar data of DP samples are not given here because the samples are opaque. As shown in Table 1, the Knoop hardness (HK1) of GC sample is 12.2 ± 0.2 GPa, which is slightly higher than 11.7 GPa (n = 1) from Krell et al. [41]. The possible reason may be the excess Al in $MgO{\cdot}1.8Al_2O_3$. Young's modulus (302 GPa) is higher than the data 295 GPa (n = 1) but lower than 303 GPa (n = 2.6) from Mitchell et al. [17], which also gives a proof that Young's modulus will be slightly increased with the increase of Al content in $MgO{\cdot}nAl_2O_3$. In addition, the changing trend of Young's modulus is well in accordance with the theoretical calculations from Tu et al. [12].

The n_D is used because it is the common way to denote an index of refraction that has been measured at the wavelength of 589.3 nm for optical materials, as it defines both surface reflections and the refraction of light inside the object. Refractive index n_D of GC samples is 1.7046 lower than 1.7161 (n = 1.0) [42], which is in accordance with Tu et al. [12]. And the Abbe's number v_D (75.8) is larger than 60.7 (n = 1.0) [42,43], which means the chromatic dispersion in n = 1.8 is smaller than that in n = 1.0.

The microstructure of $MgO{\cdot}1.8Al_2O_3$ transparent ceramic is shown in Fig. 9. The ceramic has large grain size (> 500 μm) due to the high sintering temperature (1880 °C). Hardly any residual pores could be observed, which indicates the high density of the specimen. Fig. 10 shows the in-line transmittance of the transparent $MgO{\cdot}1.8Al_2O_3$ sample, and inset gives a photo of the sample. The sample by gel-casting exhibits in-line transmittance of 77–82 % in visible region and higher than 85% in near infrared region, which is close to the theoretical limit (87.579%). In addition, the $MgO{\cdot}1.8Al_2O_3$ sample does not exhibit the absorption at around 3000 nm, which is in agreement with the literature [10,18].

4. Conclusions

In summary, non-stoichiometric $MgO{\cdot}1.8Al_2O_3$ spinel transparent ceramics were successfully fabricated for the first time by surface modification, aqueous gelcasting, and pressureless sintering followed by HIP. The obtained ceramic is highly transparent with in-line transmittance of 77–82 % in visible region, and higher than 85% in near infrared region. The anti-hydration process with stearic acid as modifying agent, Tween 80 as amphoteric surfactant, TMAH as dispersing agent before the shaping technique, is proved to be effective in passivating the surface of $MgO{\cdot}1.8Al_2O_3$ powder. The treated powders could be used to prepare stable aqueous suspensions with solid loading up to 50 vol%. The relative density of debinded bodies, linear shrinkage and relative density of samples by gelcasting on pre-sintering is superior to that of samples by dry pressing. Compared with $MgAl_2O_4$ spinel, the Young's modulus and hardness of $MgO{\cdot}1.8Al_2O_3$ have a slight increase. However, the n_D of $MgO{\cdot}1.8Al_2O_3$ is lower and Abbe's number v_D is larger than those of $MgAl_2O_4$.

Acknowledgements

This work was supported by National Key R&D Program of China (No. 2017YFB0310500) and the National Natural Science Foundation of China (Nos. 51472195, 51502219 and 51727809).

References

[1] M. Ramisetty, S. Sastri, U. Kashalikar, N. Nag, Transparent polycrystalline cubic spinels protect and defend, Am. Ceram. Soc. Bull. 92 (2) (2013) 20–25.
[2] J.A. Salem, Transparent armor ceramics as spacecraft windows, J. Am. Ceram. Soc. 96 (1) (2013) 281–289.
[3] D.C. Harris, History of development of polycrystalline optical spinel in the U.S, Window and Dome Technologies and Materials IX 5786 (2005) 1–22.
[4] M. Patterson, D.W. Roy, J.E. Caiazza, Transparent spinel development, Inorganic Optical Materials II 4102 (2000) 59–68.
[5] K.E. Green, J.L. Hastert, D.W. Roy, Polycrystalline $MgAl_2O_4$ spinel a broad band optical material for offensive environments, Window and Dome Technologies and Materials 1112 (1989) 14–74.
[6] R.W. Tustison, A.A. DiGiovanni, L. Fehrenbacher, D.W. Roy, Hard transparent domes and windows from magnesium aluminate spinel, Window and Dome Technologies and Materials IX 5786 (2005) 56–63.
[7] A. Goldstein, Correlation between $MgAl_2O_4$-spinel structure, processing factors and functional properties of transparent parts (progress review), J. Eur. Ceram. Soc. 32 (11) (2012) 2869–2886.
[8] B. Hallstedt, Thermodynamic assessment of the system MgO-Al_2O_3, J. Am. Ceram. Soc. 75 (11) (1992) 1497–1507.
[9] S.T. Murphy, C.A. Gilbert, R. Smith, T.E. Mitchell, R.W. Grimes, Non-stoichiometry in $MgAl_2O_4$ spinel, Philos. Mag. 90 (10) (2010) 1297–1305.
[10] A. Krell, K. Waetzig, J. Klimke, Influence of the structure of $MgO{\cdot}nAl_2O_3$ spinel lattices on transparent ceramics processing and properties, J. Eur. Ceram. Soc. 32 (11) (2012) 2887–2898.
[11] K. Waetzig, A. Krell, The effect of composition on the optical properties and hardness of transparent Al-rich $MgO{\cdot}nAl_2O3$ spinel ceramics, J. Am. Ceram. Soc. 99 (3) (2016) 946–953.
[12] B. Tu, H. Wang, X. Liu, W. Wang, Z. Fu, Theoretical predictions of composition-dependent structure and properties of alumina-rich spinel, J. Eur. Ceram. Soc. 36 (4) (2016) 1073–1079.
[13] A. Goldstein, A. Krell, Transparent ceramics at 50: progress made and further prospects, J. Am. Ceram. Soc. 99 (10) (2016) 3173–3197.
[14] M. Rubat du Merac, H.-J. Kleebe, M.M. Müller, I.E. Reimanis, Fifty years of research and development coming to fruition: unraveling the complex interactions during processing of transparent magnesium aluminate ($MgAl_2O_4$) spinel, J. Am. Ceram. Soc. 96 (11) (2013) 3341–3365.
[15] A. Krell, E. Strassburger, T. Hutzler, J. Klimke, W. Chen, Single and polycrystalline transparent ceramic armor with different crystal structure, J. Am. Ceram. Soc. 96 (9) (2013) 2718–2721.
[16] A.C. Sutorik, C. Cooper, G. Gilde, M. Cinibulk, Visible light transparency for polycrystalline ceramics of $MgO{\cdot}2Al_2O_3$ and $MgO{\cdot}2.5Al_2O_3$ spinel solid solutions, J. Am. Ceram. Soc. 96 (12) (2013) 3704–3707.
[17] T.E. Mitchell, Dislocations and mechanical properties of MgO-Al_2O_3 spinel single crystals, J. Am. Ceram. Soc. 82 (12) (1999) 3305–3316.
[18] N. Fukatsu, N. Kurita, H. Shiga, Y. Murai, T. Ohashi, Incorporation of hydrogen into magnesium aluminate spinel, Solid State Ionics 15 (2002) 809–817.
[19] D. Lenaz, H. Skogby, F. Nestola, F. Princivalle, OH incorporation in nearly pure $MgAl2O_4$ natural and synthetic spinels, Geochim. Cosmochim. Acta 72 (2) (2008) 475–479.
[20] I. Ganesh, S.M. Olhero, A.H. Rebelo, J. Ferreira, Formation and densification behavior of $MgAl_2O_4$ spinel: the influence of processing parameters, J. Am. Ceram. Soc. 91 (6) (2008) 1905–1911.
[21] A. Krell, T. Hutzler, J. Klimke, A. Potthoff, Fine-grained transparent spinel windows by the processing of different nanopowders, J. Am. Ceram. Soc. 93 (9) (2010)

2656–2666.
[22] X. Liu, H. Wang, B. Tu, W. Wang, Z. Fu, Highly transparent $Mg0.27Al_{2.58}O_{3.73}N0.27$ ceramic prepared by pressureless sintering, J. Am. Ceram. Soc. 97 (1) (2014) 63–66.
[23] D. Guo, K. Cai, L. Li, Z. Gui, Application of gelcasting to the fabrication of piezoelectric ceramic parts, J. Eur. Ceram. Soc. 23 (7) (2003) 1131–1137.
[24] J. Yang, J. Yu, Y. Huang, Recent developments in gelcasting of ceramics, J. Eur. Ceram. Soc. 31 (14) (2011) 2569–2591.
[25] I. Ganesh, D.C. Jana, S. Shaik, N. Thiyagarajan, An aqueous gelcasting process for sintered silicon carbide ceramics, J. Am. Ceram. Soc. 89 (10) (2006) 3056–3064.
[26] I. Ganesh, N. Thiyagarajan, D.C. Jana, P. Barik, G. Sundararajan, An aqueous gelcasting route to dense β-$Si_4Al_2O_2N_6$-$0.5SiO_2$ ceramics, J. Am. Ceram. Soc. 91 (5) (2008) 1566–1571.
[27] Y. Shimizu, H. Arai, T. Seiyama, Theoretical studies on the impedance-humidity characteristics of ceramic humidity sensors, Sens. Actuators 7 (1) (1985) 11–22.
[28] I. Ganesh, Aqueous slip casting of $MgAl2O_4$ spinel powder, Bull. Mater. Sci. 34 (2) (2011) 327–335.
[29] I. Ganesh, S. Olhero, P. Torres, J. Ferreira, Gelcasting of magnesium aluminate spinel powder, J. Am. Ceram. Soc. 92 (2) (2009) 350–357.
[30] I. Ganesh, G. Sundararajan, J.M.F. Ferreira, Aqueous slip casting and hydrolysis assisted solidification of $MgAl2O_4$ spinel ceramics, Adv. Appl. Ceram. 110 (2) (2013) 63–69.
[31] S. Olhero, I. Ganesh, P. Torres, J. Ferreira, Surface passivation of $MgAl_2O_4$ spinel powder by chemisorbing H_3PO_4 for easy aqueous processing, Langmuir 24 (17) (2008) 9525–9530.
[32] M. Egashira, Y. Shimizu, S. Takatsuki, Chemical surface treatments of aluminium nitride powder suppressing its reactivity with water, J. Mater. Sci. Lett. 10 (17) (1991) 994–996.
[33] H. Gu, X. Chen, H. Jiang, C. Zhang, S. Liu, Optimal broadband Mueller matrix ellipsometer using multi-waveplates with flexibly oriented axes, J. Opt. 18 (2) (2016) 1–11.
[34] S. Liu, X. Chen, C. Zhang, Development of a broadband mueller matrix ellipsometer as a powerful tool for nanostructure metrology, Thin Solid Films 584 (15) (2015) 176–185.
[35] C.V. Nikiforidis, V. Kiosseoglou, Competitive displacement of oil body surface proteins by tween 80 – effect on physical stability, Food Hydrocoll. 25 (5) (2011) 1063–1068.
[36] R.A. Nyquist, P.O. Kagel, C.L. Putzig, M.A. Leugers, The handbook of infrared and Raman spectra of inorganic compounds and organic salts, Vib. Spectrosc. 14 (2) (1997) 303–304.
[37] V. Erukhimovitch, Y. Mordekoviz, S. Hayun, Spectroscopic study of ordering in non-stoichiometric magnesium aluminate spinel, Am. Min. 100 (8-9) (2015) 1744–1751.
[38] M. Ishii, J. Hiraishi, T. Yamanaka, Structure and lattice vibrations of Mg-Al spinel solid solution, Phys. Chem. Miner. 8 (2) (1982) 64–68.
[39] Y. Wan, Y. Wang, Q. Zhang, Z. Wang, Low-friction performance of stearic acid modification of nano-textured ZnO coating, Nanosci. Nanotechnol. Lett. 4 (9) (2012) 910–913.
[40] A. Krell, J. Klimke, Effects of the homogeneity of particle coordination on solid-state sintering of transparent alumina, J. Am. Ceram. Soc. 89 (6) (2006) 1985–1992.
[41] A. Krell, A. Bales, Grain size-dependent hardness of transparent magnesium aluminate spinel, Int. J. Appl. Ceram. Technol. 8 (5) (2011) 1108–1114.
[42] RefractiveIndex. INFO, $MgAl_2O_4$ (Magnesim aluminate, spinel). https://refractiveindex.info/?shelf=main&book=$MgAl_2O_4$&page=Tropf/, 2018 (Accessrd 3 January 2018).
[43] A. Krell, T. Hutzler, J. Klimke, Transmission physics and consequences for materials selection, manufacturing, and applications, J. Eur. Ceram. Soc. 29 (2) (2009) 207–221.